Composites: Part A 181 (2024) 108138

Contents lists available at ScienceDirect

Composites Part A

journal homepage: www.elsevier.com/locate/compositesa

Direct electrospinning of short polymer fibers: factors affecting size and quality

Daniel P. Ura, Urszula Stachewicz *

Faculty of Metals Engineering and Industrial Computer Science, AGH University of Krakow, 30-065 Kraków, Poland

ARTICLE INFO

Keywords:
Short fibers
Electrospinning
PMMA
Homogenization

ABSTRACT

The growing demand for lightweight and robust materials drives the development of polymer-based and fiber-reinforced composites. Here, using short fibers offers several advantages; however, currently employed methods for producing short fibers, such as homogenization, result in a wide dispersion of dimensions in the produced fibers, which is an undesirable effect in composite materials. In this study, electrospinning is used to produce polymer short fibers directly. This research highlights, for the first time, the differences in the electrospinning process dynamics between short and continuous fibers. By adjusting parameters: voltage and distance, we control dimensions of short fibers below 1 μm in diameter and around 4 μm in length to a few microns in diameter and approximately 14 μm in length. Direct electrospinning of short fibers offers significant advantages, including a narrow size distribution and reproducibility compared to chopped continuous fibers with homogenization.

1. Introduction

The continuously growing need for light and high-strength materials is pushing the development of polymer-based composites, especially reinforcements and impregnation strategies. Here, the vast role is played by fiber-reinforced composites (FRCs), advanced materials composed of a polymer matrix and high-strength fibers, like carbon, glass, nylon, or aramid, that are aligned to provide mechanical strength, stiffness, and toughness.[1] FRCs are widely used in aerospace, automotive, and bio-industry due to their mechanical, thermal, or biological properties.[2,3] Additionally, biodegradable polymer FRCs reinforced with natural fibers like cellulose, chitin, and lignin are a sustainable alternative to conventional composites, still keeping high mechanical strength and biocompatibility, making them attractive for biomedical applications such as tissue engineering, drug delivery, and implants.[4–9] FRCs can be divided into two types according to the fiber used: continuous and short fibers.[10,11] Short fibers offer several advantages over continuous fibers in specific applications. For example, short fibers can be uniformly dispersed throughout a polymer matrix, leading to a homogeneous composite material and improving mechanical properties, including increased toughness and impact resistance, making them suitable for high-performance applications like multilayer armor systems.[12–14] Short fibers are often more cost-effective than continuous fibers and can produce composite materials at a lower cost.[15] However, the methods currently used to produce short fibers, such as homogenization or ultrasonication, result in wide dispersion in the dimensions of produced fibers, which is an undesirable effect in composite materials.[16,17].

Electrospinning is a technique used to produce strong and durable continuous polymer fibers for various applications, including composites.[18–20] It involves an electric field to draw a polymer solution from a needle to a collector, producing continuous fibers ranging from nanometers to micrometers.[21,22] Approaches for producing fibers via electrospinning include controlling solution properties like the type of solvents, concentration, viscosity, conductivity, and surface tension or adjusting electrospinning parameters such as voltage, electrical polarity, polymer solution flow rate, and distance between needle and collector to influence fiber morphology and dimensions.[23–25] Electrospun continuous fibrous mats are often mechanically cut to produce short polymer fibers, resulting in a significant variation in fiber dimensions and aspect ratio. However, some literature shows that short fibers can be manufactured via electrospinning.[26–29] Short fiber size produced through electrospinning can be controlled by adjusting process parameters such as applied voltage, nozzle-to-collector distance, electric field strength, and polymer flow rate.[30] Additionally, polymer solution concentration, molecular weight, viscosity, and type of solvents (good or

* Corresponding author.
E-mail address: ustachew@agh.edu.pl (U. Stachewicz).

https://doi.org/10.1016/j.compositesa.2024.108138
Received 24 October 2023; Received in revised form 21 February 2024; Accepted 9 March 2024
Available online 12 March 2024

θ-solvent) are critical factors that affect short fiber size, for example, higher concentrations resulting in a larger diameter of fibers.[27,28,31] The direct way of producing short fibers via electrospinning is the one-step manufacturing and easy scale-up method. On the other hand, polymer selection maybe limited to obtain short fibers. However, there is still a lack of comprehensive mapping of electrospinning parameters to figure out the most effective method for producing short fibers with well-controlled dimensions and the highest quality of polymer fibers.

We selected poly(methyl methacrylate) (PMMA) as a model polymer for this study to verify the best ways of directly produce short fibers via electrospinning. PMMA is a transparent and stiff polymer commonly used as a matrix in composite materials due to its environmental stability and density.[32] Importantly, PMMA is biocompatible and frequently used in many biomedical applications such as contact lenses, dental fillings and implants.[32,33] Additionally, PMMA is using in composites due to its high strength-to-weight ratio and resistance to impact.[34,35] It is often combined with other materials such as carbon fibers, fiberglass, and epoxy resins to create lightweight and durable composites for aircraft, marine, and automotive industries.[36–38] PMMA improves strength and stiffness in composites while maintaining excellent optical clarity.[39–41] However, it has low elongation and high brittleness, especially when exposed to longitudinal force in fiber form, which can cause fragmentation into short fibers.[30] Due to mentioned properties, PMMA short fibers can be used to reinforce various types of composites or hydrogels.

Therefore, in this study, we produced short fibers by homogenization, indirectly, and directly by electrospinning. Notably, based on detailed observation of the electrospinning process using a high-speed camera, we point out the differences in polymer jet behavior during the production of continuous and short fibers. Importantly, we show the strategies to control short fiber dimensions by changing applied voltage, nozzle-to-collector distance, and polymer solution flow rate in electrospinning and the potential future application of short fibers produced by electrospinning. It is the first time the directly electrospun fibers were compared to the commonly chopped and homogenized short fibers. We provide a comprehensive and unique analysis for producing short polymer nano- and microfibers with a very narrow size distribution.

2. Experimental methods

2.1. Polymer solution

The continuous fiber was produced using a 12 wt% of poly(methyl methacrylate) (PMMA, M_w = 350 000 g·mol^{-1}, Sigma Aldrich, UK) dissolved in dimethylformamide (DMF). Solutions were stirred at 700 rpm for 2.5 h on a hot plate set at 55 °C (IKA RCT basic, Germany). To produce short fibers, 52 wt% polymer solution of PMMA (M_w = 15 000 g·mol^{-1}, Sigma Aldrich, UK) powder was dissolved in DMF (Sigma Aldrich, UK).

2.2. Electrospinning of fibers

Continuous and short polymer fibers were produced via electrospinning using apparatus EC-DIG with a single nozzle system (stainless-steel nozzle with 0.51 mm inner and 0.82 mm outer diameter, 21G x 1 1/2″) and climate control (SKE Research Equipment, Italy) at T = 25 °C and 40 % relative humidity (RH). All electrospinning parameters are summarized in Table 1. Electrospinning parameters were selected for the minimum, middle (in-between), and maximum values where the process showed stability (non-drying of the needle, discontinuity of the polymer jet, etc.) to produce short fibers. Fibers were deposited on a stainless drum collector covered with Al foil rotating at 24 rpm for 30 min for short fibers and 180 min for continuous fibers. After fabrication, the fibers were put in stable atmospheric conditions T = 25 °C and 30 % RH for 7 days to evaporate the solvent.

Table 1
Electrospinning parameters used to produce short and continuous PMMA fibers. Based on the information in the introduction (effect of electric field strength), the results were normalized for samples 1–5 (change in applied voltage and distance). For this purpose, an equation for the electric field strength E was used: $E = \frac{U}{Y}$, where U is the applied voltage, and Y is the nozzle-to-collector distance. [25] Q is the flow rate of the polymer solution.

Type of fibers	Sample Name	*U* [kV]	*Y* [cm]	Q [ml·h^{-1}]	*E* [kV·cm^{-1}]
Short	SF1	10	22	0.5	0.45
	SF2	15	22	0.5	0.68
	SF3	23	22	0.5	1.04
	SF4	23	15	0.5	1.53
	SF5	23	27	0.5	0.85
	SF6	23	22	0.1	1.04
	SF7	23	22	1	1.04
Continuous	F	23	22	4	1.04

2.3. Homogenization of continuous fibers

Continuous fibers were homogenized using an immersion disperser (Polytron PT 10–35 GT, Kinematica AG, Malters, Switzerland) with a "w-design" blade (PT-DA 12/2WEC-F154, Kinematica AG, Malters, Switzerland). Then, 0.5 wt% of the PMMA fibers were immersed in a mixture of deionized water and ethanol in a 9:1 ratio for 5 min.[42] Next, fibers were homogenized for 10, 30, and 60 min at 10 000 rpm.

2.4. High-speed imaging of electrospinning polymer jet

Slow-motion video of continuous and short fibers electrospinning near a bending instability region of a polymer jet was performed using a high-speed camera (Chronos CR14-1.0, Krontech, Canada) with a macro lens (EF-S, 60 mm f/2.8 Macro, Canon, Japan). Recording speed and resolution were 5413 fps and 495 × 500 pixels.

2.5. Scanning electron microscopy (SEM)

The fiber morphology was investigated using SEM (Merlin Gemini II, ZEISS, Germany) at 2.5 kV accelerating voltage, 110 pA current, and a working distance between 4 and 9 mm. Prior to the SEM analysis, samples were coated with a 5 nm thick Au layer using a sputter coater (Quorum Q150RS, Quorum Technologies Ltd., UK).

2.6. Thermal analysis and fourier-transform infrared spectroscopy (FT-IR)

Thermal characterization was done using differential scanning calorimetry (DSC, Model 3, Mettler Toledo, USA) at a heating rate of 10 °C·min^{-1} in the −20 to 220 °C temperature range. Measurements were conducted in an Ar atmosphere for the sample placed in the Al pan. Average glass transition temperatures were determined based on 3 measurements from 1st heating curves, see Fig. S1 in supporting information (SI).

The chopped and short fibers were analyzed using FTIR (Nicolet iS 5, Thermo Fisher Scientific, USA), by the attenuated total reflection (ATR) technique with the diamond crystal. During measurements, the spectra were 64 repeated over the 500–4000 cm^{-1} wavenumber range, with a resolution of 4 cm^{-1}. All spectra have been normalized, atmospheric corrected, offset, and background subtracted for visual clarity, as shown in Fig. S1 in SI.

2.7. Statistical analysis

Fiber diameter (D_f) and length (L_f) for PMMA were measured from SEM images and analyzed using ImageJ software (version 1.51, Fiji, USA). The aspect ratio was calculated for each fiber separately. The

average (arithmetic mean) fiber diameter, length, and ratio values were calculated from 100 measurements, and the error was based on the standard deviation. The statistical analysis of the fiber morphology was performed using Student's *t*-test with OrginPro (2022 SR1, OriginLab, USA) software. For all tests, the significance was set at $p < 0.05$. All average values are summarized in Table S1 in SI. Graph clustering was prepared using a centroid function (eclipse) with a confidence level (prediction) set to 80 in OrginPro software.

3. Results and discussion

3.1. Polymer jet during the electrospinning process of short and continuous fibers

The dynamic process of electrospinning and polymer jet formation in the electric field between the nozzle and counter electrode was captured using a high-speed camera. We were able to record the difference between the electrospinning processes of continuous and short fibers, see the camera images in Fig. 1, which shows a stop frame from an electrospinning jet near a bending instability region. The full recording is available as Video 1 in SI. Similar process parameters for continuous and short fibers electrospinning were used to compare polymer jet bending during fiber production, see Table 1. Fig. 1 **(a)** shows a straight section of the polymer jet bending instability and whipping jet, all indicated with the colored arrows, which is unique for the electrospinning of continuous polymer fibers.[22,25,43] For short fibers electrospinning, see Fig. 1 **(b)**, a straight section of the jet is evident, as well as bending instability. However, no part of the whipping jet is visible. Clearly, the stop-frame images of the electrospinning process close to the region of instability showed a significantly different behavior of the polymer jet depending on the type of fibers produced.

Previously, Fathona and Yabuki presented an image of jet ejection from a needle tip and a schematic explanation of the short electrospun fiber formation mechanism.[28] It was proposed that the main factor leading to the production of short fibers was the maximum force a polymer solution jet could withstand while being stretched before breaking. This force depends on the polymer macromolecular architecture (linear or branched), thus, polymer chain entanglement, solution concentration, and polymer–solvent interaction in the solution forming the jet.[44] Additionally, the lower molecular weight of the polymer led to lower mechanical properties of the jet due to decreased entanglement of chains.[45,46] In our case, electrospinning performed with lower molecular weight PMMA' solution shows a region where polymer jet breaks and short fibers formations are visible, see Fig. 1 **(b)** and red arrows. Similarly, Greenfeld and Zussman *et al.* obtained a short fiber by selecting a PMMA with 15 000 g·mol^{-1} molecular weight and ~ 30 % polymer concentration dissolved in 1:1 chloroform/DMF in the solution used for electrospinning.[31] The authors obtained continuous fibers from PMMA with 101 000 and 350 000 g·mol^{-1} dissolved in 1:1 chloroform/DMF and polymer concentrations between 3 and 40 wt%. Depending on the polymer structure: linear or branched, its molar mass, concentration in solution, and solvent quality, short nanofibers may be formed in/from semi-dilute entangled solutions. The entanglement of polymer chains is highly effective in transferring mechanical stress. When the polymer network is not highly entangled, the high strain rate caused by the electrostatic field can stretch and disentangle chains from the network and break the jet into short segments. Entanglement loss is governed by two opposing variables: the entanglement number and chain relaxation time. Both depend on the polymer chain's degree of polymerization N (number of monomer units in the polymer). The entanglement number, so the number of topological constraints along the chain, scales with N, while the chain relaxation time in an entangled network scale with N^3. When the jet strain rate is low, rapid relaxation of the network prevents entanglement loss, and viscosity is dominant. However, at high strain rates, relaxation is not sufficiently fast, and elasticity is dominant, making chain extension and disentanglement possible. Hence, lower N, shorter chain, thus lower molecular weight, reduces entanglement and relaxation time. Therefore, the net effect on entanglement loss relies upon the strain rate of the polymer jet in an electrical field. At the same time, the rapid solvent evaporation characteristic of electrospinning partially solidifies the jet, retards entanglement loss and jet breaking. It prevents the jet segments from contracting back into droplets by relaxation and surface tension. Generally, the probability of short nanofiber fabrication during electrospinning highly depends on polymer concentrations (polymer volume fraction), polymer chain entanglement, type of solvents (good or θ-solvent), and electric field strength value.[31] In the case of this work, electrospinning of continuous and short fibers was performed for PMMA using two different molecular weights: high reaching 350 000, and low having 15 000 g·mol^{-1}, dissolved in the DMF. This way, we could verify the effect of molecular weight on the production of short fibers.

3.2. Homogenization of continuous fibers

Continuous PMMA fibers were successfully fabricated, as shown in Fig. 2 **(a)**, in the stable electrospinning process, as the microscopy

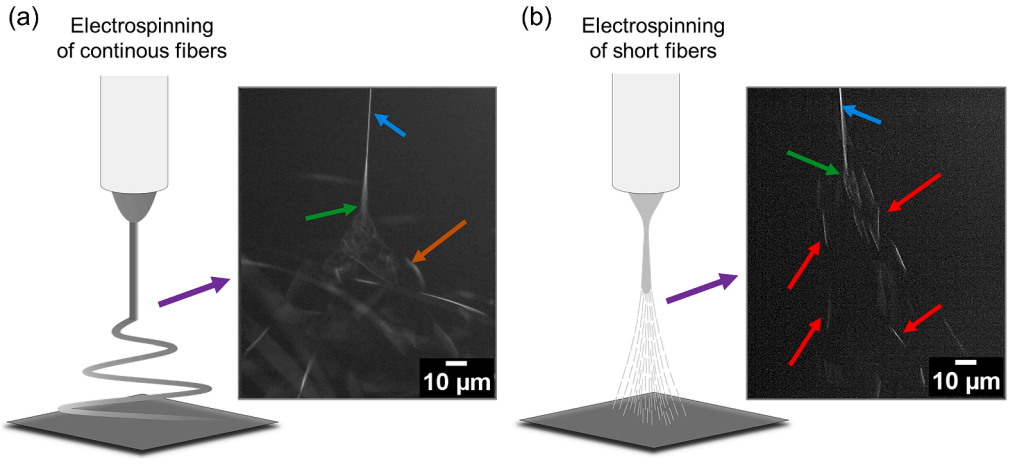

Fig. 1. Schematic of the electrospinning process and high-speed camera imaging from polymer jet near a bending instability region of (a) – continuous and (b) – short fibers. Colored arrows were used to differences at the electrospinning jets: blue - straight section of jet; green - polymer jet bending instability, orange - whipping jet and red arrow – polymer jet break into short fibers. (For interpretation of the references to colour in this figure legend, the reader is referred to the web version of this article.)

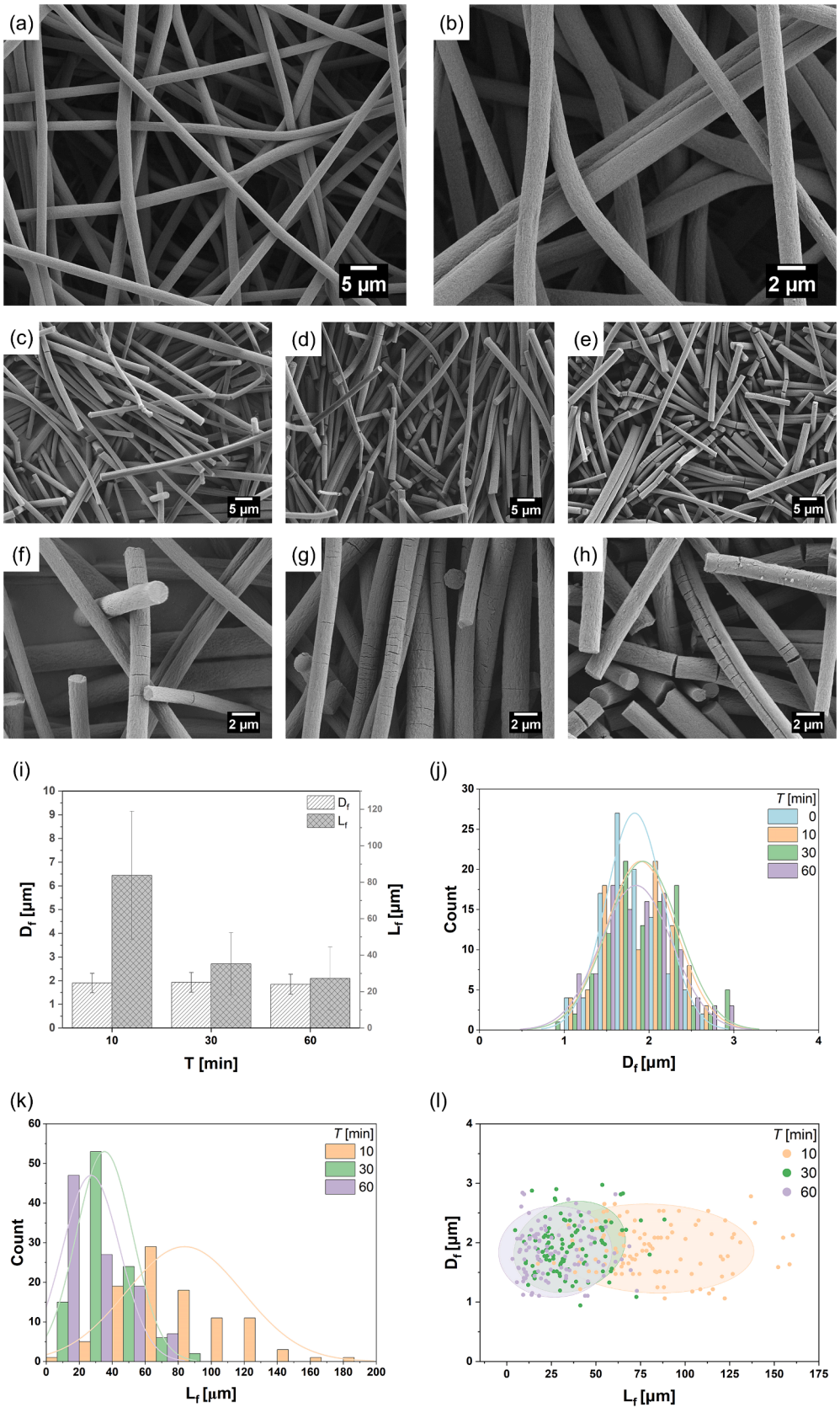

Fig. 2. SEM images of chopped fibers produced with different homogenization times: pristine continuous fibers – (a, b) 0 min; (c) 10 min; (d) 30 min; (e) 60 min. SEM images of microcracks observed at short fibers produced with different homogenization times: (f) 10 min; (g) 30 min; (h) 60 min. Bar graph (i) and histograms of fiber diameter (j) and length distribution (k) produced with specific homogenization time (T). The relation between chopped fiber diameter and length made with different homogenization times is presented in cluster plot (l). Sample $T = 0$ (b) is a PMMA continuous fiber.

analysis did not show any discontinuities or beads in the structure of fibers. The average fiber diameter (D_f) was 1.83 ± 0.33 μm. To create a chopped fiber from the electrospun mat, we homogenized continuous PMMA fibers at 3 different process times: 10-, 30-, and 60-min. SEM images of chopped fibers after homogenization can be found in Fig. 2 **(c - h)**. The average fiber diameters were approximately 1.90 ± 0.41 μm for all set processing times. The length of chopped fibers was successive, 83.80 ± 35.11 μm for 10 min, 35.28 ± 17.03 μm for 30 min, and 27.23 ± 17.30 μm for 60 min. The average aspect ratio was 47.04 ± 25.77 (10 min), 19.00 ± 10.24 (30 min), and 15.51 ± 11.03 (60 min), respectively. Fig. 2 **(i - l)** presents the bar graph, histograms, and cluster plot of fiber dimensions and ratio. All results for homogenized fibers were summarized in Table S1 in SI.

Homogenization parameters such as time, blade rotation speed, and the type of medium used for homogenization affect the chopped fiber morphology and length.[47] However, the homogenization in the mixture of water and ethanol used in this study did not affect the fiber diameter. Increasing homogenization time decreased chopped fibers' length and aspect ratio, as shown in Fig. 2 **(i).** Similar results were observed for polystyrene (PS) continuous fibers, where homogenization did not affect morphology or diameter but the length of fibers.[48] The mean length and aspect ratio was 11 ± 17 μm and 18.54 after 3 h of

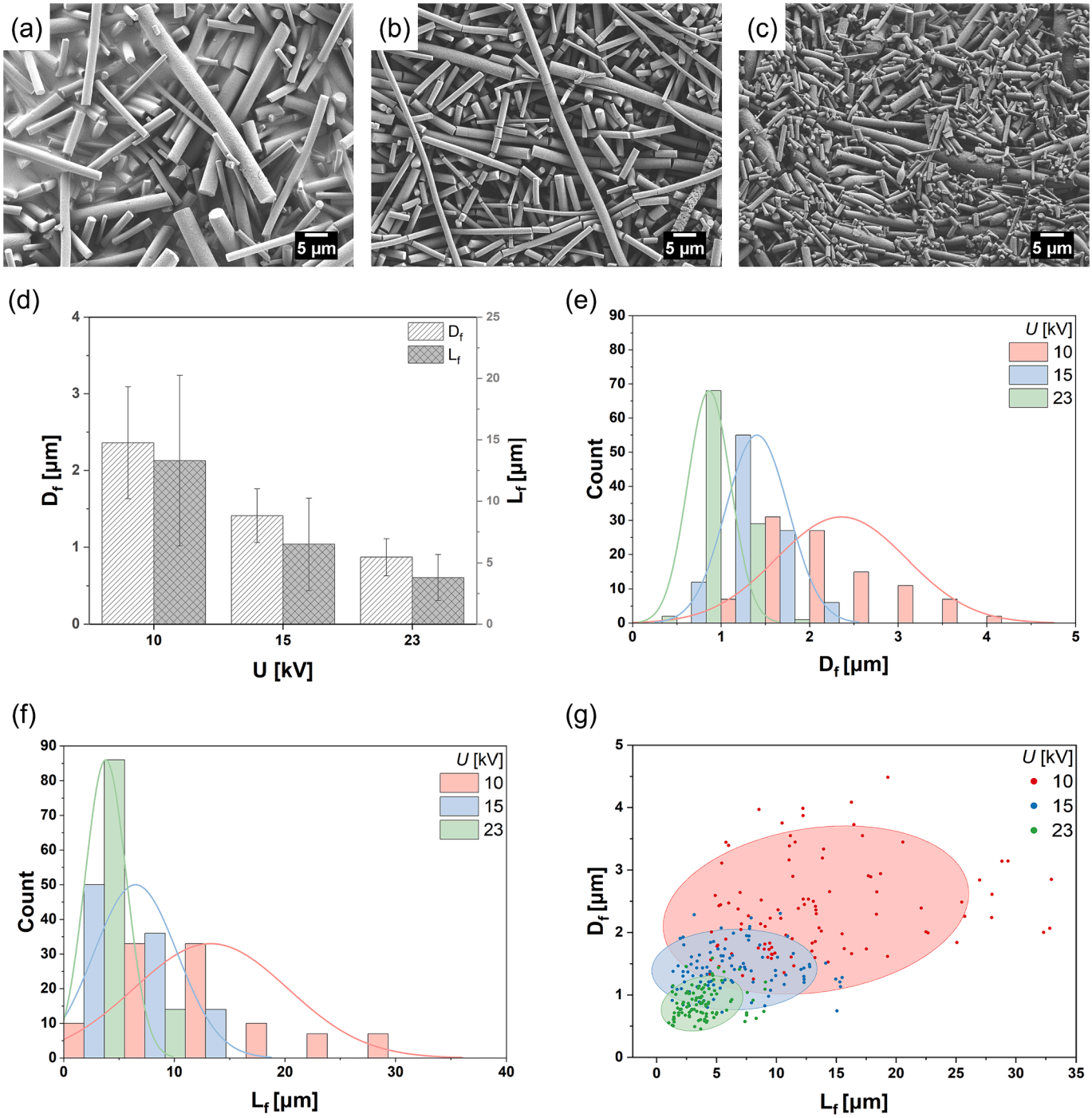

Fig. 3. SEM images of short fibers produced with different applied voltages: (a) 10 (SF1), (b) 15 (SF2), and (c) 23 kV (SF3) at the constant flow rate, Q and distance nozzle-to-collector, Y. Bar graph of D_f and L_f to applied voltage U - (d). Fiber diameter (e) and length (f) distribution histograms and the relation between fiber length and diameter of short fibers in the form of cluster plot (g) produced with different applied voltage.

homogenization. Xi *et al.* produced polyacrylonitrile (PAN) fibers with a length from 3 to 7 μm and an aspect ratio of from 7.5 to 23.3 by grinding for 1 h and ultrasonication for 10 min.[49] In other work, PAN continuous fibers were mechanically cut at 23000 rpm for 10 min, resulting in 442 ± 171 μm in length and 401.81 in aspect ratio.[50] Polyacrylic acid (PAA) fibers had 0.3 μm in diameter, 1 min of cutting delivered fibers 87 ± 53 μm in length, and 271.8 aspect ratio.[51] One of the disadvantages of homogenizing polymer fibers in the case of our electrospun PMMA was microcracks on the surface of the chopped fibers, which were revealed by SEM analysis. The cracking of fibers resulted from the mechanical cutting process, see Fig. 2 **(f – h)**.[52,53].

3.3. Electrospinning of short fibers

Short PMMA fibers were successfully fabricated using electrospinning with different process parameters, see Figs. 3-6. This section discusses the effects of process parameters: applied voltage, nozzle-to-collector distance, electric field strength, and polymer flow on the diameter, length, and aspect ratio of short electrospun fibers.

3.3.1. Effect of applied voltage effect on the short fibers

In electrospinning, the main force that creates a polymer jet is the electrostatic force. It can be enhanced by increasing the electrical field strength (voltage applied and nozzle-to-collector distance) and changing an electrical polarity that may change the charge density of polymer solutions depending on the presence of cations and anions.[54–56] So, suppose the electrostatic force is high enough to exceed the maximum force that a polymer solution jet can withstand before breaking. In that case, fibers are deposited in the form of short fibers. For this work, as mentioned earlier, it was possible to produce short fibers by using an appropriate solution, the specific molecular weight, and the polymer concentration, thus causing entanglement loss.[31] Additionally, increasing the applied voltage causes an increasing electric force (Maxwell stress), thus changing the dynamics of the process and the rising force responsible for breaking the jet.[31,57] Consequently, greater force acts on the jet, causing a reduction of fiber diameter and breaking fibers into shorter pieces by reducing fiber length, which was observed in this work, see Fig. 3 and Table S1 in the SI. Short electrospun PMMA fibers were fabricated using 10, 15, and 23 kV applied voltage, maintaining the same polymer solution flow rate and distance, as shown in Fig. 3 **(a)**. Average short fiber diameters and length were successive, 2.36 ± 0.73 and 13.30 ± 6.95 μm for 10 kV, 1.41 ± 0.35 and 6.49 ± 3.75 μm for 15 kV, and 0.87 ± 0.24 and 3.79 ± 1.86 μm for 23 kV. The average aspect ratio of short fiber was 5.93 ± 3.11 (10 kV), 4.90 ± 3.32

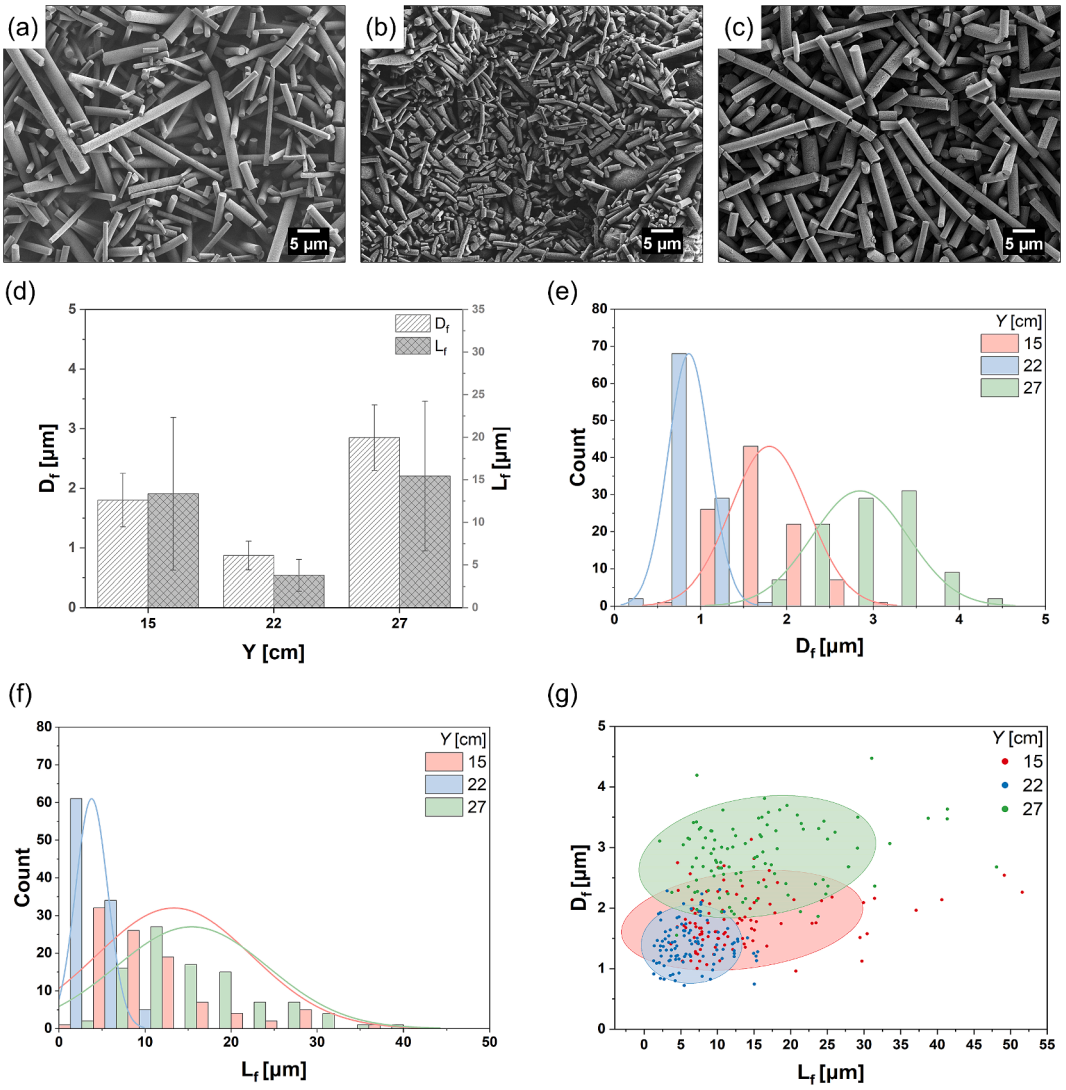

Fig. 4. SEM images of short fibers produced with: (a) 15 (SF4), (b) 22 (SF3), and (c) 27 (SF5) cm nozzle-to-collector distances at constant applied voltage, *U* and flow rate, *Q*. Bar graph of average D_f and L_f to distance *Y* - (d). Fiber diameter (e) and length (f) distribution histograms and the relation between fiber length and diameter of short fibers in the form of cluster plot (g) for different distances.

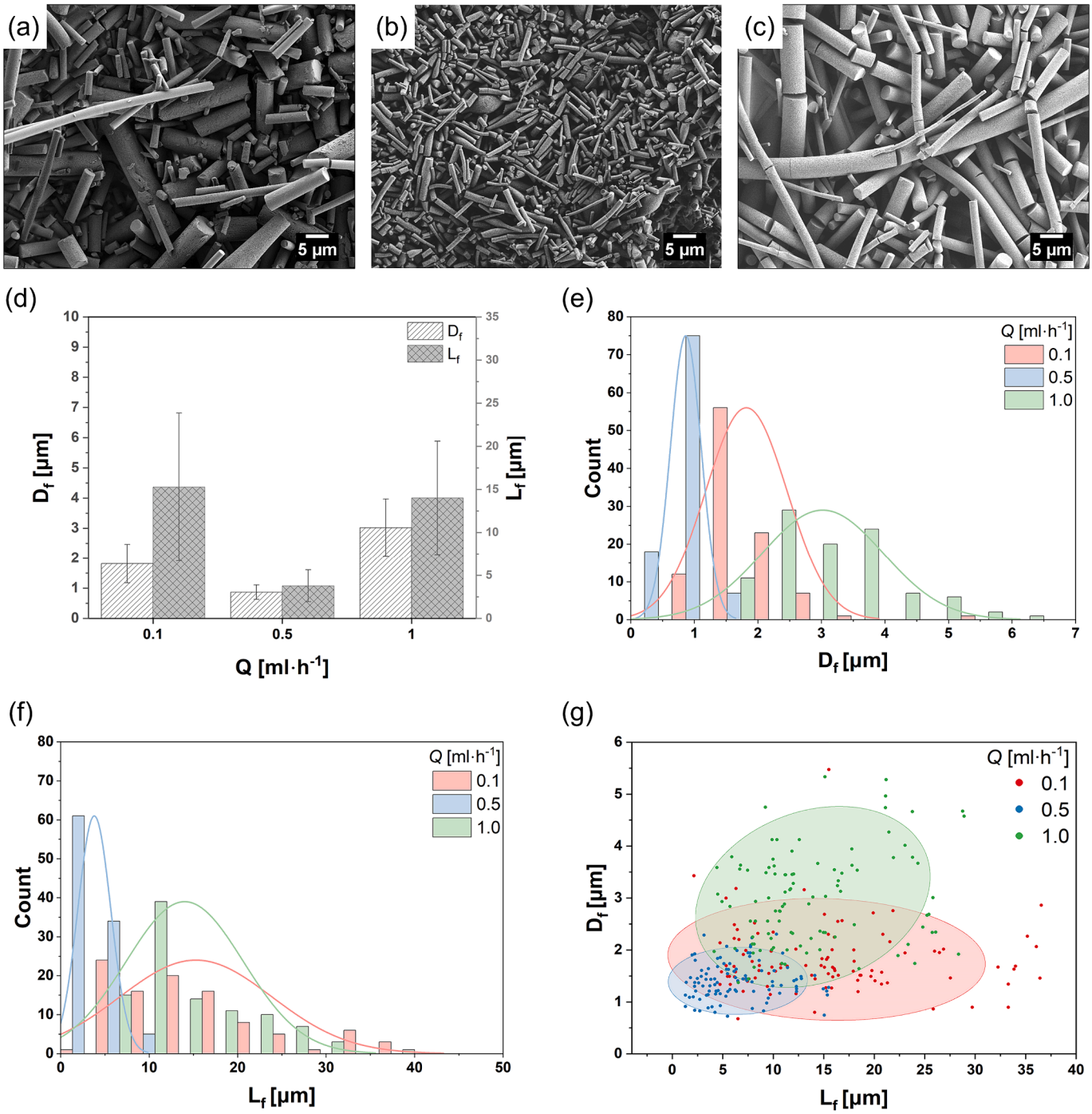

Fig. 5. SEM micrographs of short fibers produced with different flow rates: (a) 0.1 (SF6), (b) 0.5 (SF3), and (c) 1.0 ml·h^{-1} (SF7) at the constant applied voltage, *U* and distance nozzle-to-collector, *Y*. Bar graph of D_f and L_f for different flow rates *Q* (d). Short fiber diameter (e) and length (f) distribution histograms for 0.1, 0.5, and 1.0 ml·h^{-1}. Relation between fiber length to the diameter of short fibers produced by different flow rates in cluster plot (g).

(15 kV), and 4.58 ± 2.46 (23 kV), respectively. The bar graph, histograms, and cluster plot of fiber diameter, length, and aspect ratio were presented in Fig. 3 **(d – e).** All collected data were summarized in Table S1 in the SI. By varying the applied voltage, it has been possible to produce PMMA short fibers with diameters ranging from 0.8 to 2.4 µm and lengths from 3.8 to 13.3 µm, which is unique compared to other methods. In other work, electrospun PMMA short fibers reached lengths of approximately 1000 µm with a wide size distribution, which is ~ 200 times higher than our results.[31] Similar observations were for the PMMA and cellulose acetate (CA) aspect ratio, where we obtained ~ 5 times much lower value than in the previous studies, reaching more than 20 and even up to 300.[28,31,58].

3.3.2. *Effect of nozzle-to-collector distance on short fibers*

As with the applied voltage, the distance between the needle and the collector significantly affects the dimensions of the short PMMA fibers. As the distance changes, the electrical force acting on the polymer jet varies.[25] This work fabricated short PMMA fibers using the three nozzle-to-collector distances: 15, 22, and 27 cm, as shown in Fig. 4. SEM analysis did not show any discontinuities or beads in the structure of fibers. The bar graph, histograms, and cluster plot of fiber diameter, length, and length-to-diameter ratio were presented in Fig. 4 **(d – g)**.

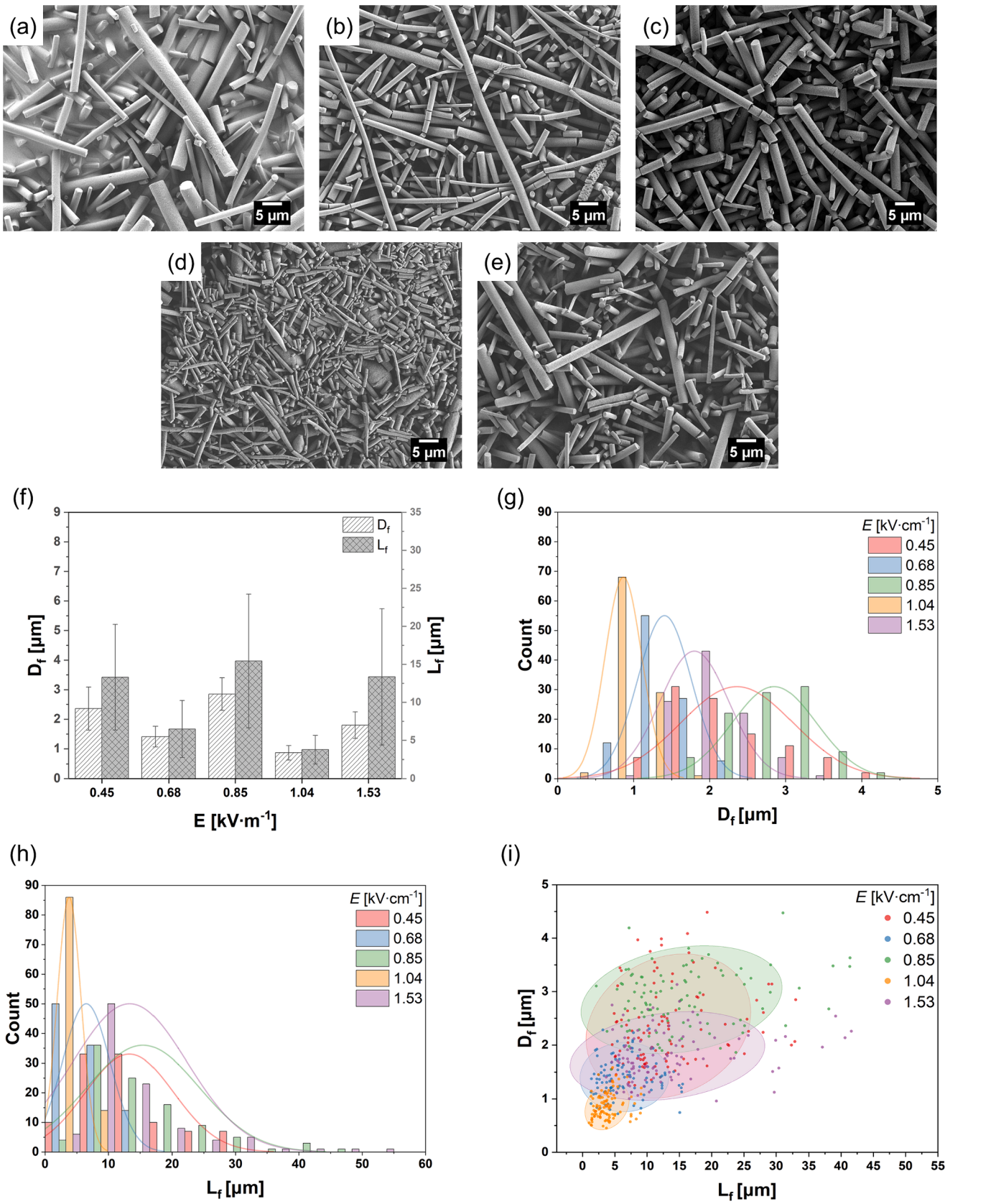

Fig. 6. SEM images of short fibers produced with (a) 0.45 (SF1), (b) 0.68 (SF2), (c) 0.85 (SF5), (d) 1.04 (SF3), and (e) 1.53 (SF4) kV·cm^{-1} electrical field strength. Bar graph of average D_f and L_f to distance Y - (f). Fiber diameter (g) and length (h) distribution histograms and the relation between fiber length and diameter of short fibers in the form of cluster plot (i) for different electrical field strengths.

Average diameters and lengths were successive: 1.80 ± 0.45 and 13.35 ± 8.97 μm for 15 cm, 0.87 ± 0.24 and 3.79 ± 1.86 μm for 22 cm, and 2.85 ± 0.55 and 15.44 ± 8.80 μm for 27 cm. The average aspect fiber ratio was 7.60 ± 4.78 (15 cm), 4.58 ± 2.46 (22 cm), and 5.51 ± 3.06 (27 cm), respectively. All average diameters, lengths, and aspect ratios of fiber produced with different distances were summarized in Table S1 in the SI.

The smallest fibers, ~0.8 μm in diameter and ~ 3.8 μm in length, were obtained at a 22 cm distance between the nozzle and the collector. Interestingly, comparable results about the electrospinning of continuous fibers can be found in other works. The fiber diameter suddenly drops for a certain distance from the collector and then increases again for a higher distance.[54,59,60] However, the explanation for this phenomenon is still lacking. When reducing the electrical field strength, so extending the distance between electrodes under the same electrical potential, the electrical forces are negligible, and therefore, insignificant elongation of the polymer jet, often indicated by reducing the diameter of the jet, happens. Thus, the diameter of fibers is controlled by the flow rate and nozzle diameter. The effect of nozzle-to-collector distance on the aspect ratio is not visible. Nevertheless, despite the lack of differences in aspect ratio between samples produced at 15, 22, and 27 cm, a notable change in the dimensions is apparent. For example, at 27 cm, the average short fiber dimensions are ~ 3 μm in diameter and ~ 15 μm long. However, for 22 cm, the size is 1 μm in diameter and 4 μm long, resulting in approximately 3 times smaller fibers with the same aspect ratio.

3.3.3. Flow rate effect on short fibers size

By controlling polymer solution flow rates, it has been possible to produce PMMA fibers with diameters from around 0.87 to 3.02 μm and lengths from 3.79 to 15.28 μm. In electrospinning, the diameter of continuous fibres decreased with a reduced polymer flow rate.[61,62] In our study, we successfully fabricated short PMMA fibers using the different polymer flow rates: 0.1, 0.5, and 1.0 ml·h^{-1}, as shown in Fig. 5. SEM analysis did not show any discontinuities or beads in the structure of fibers. The average diameters and lengths of obtained short fibers were 1.82 ± 0.64 and 15.28 ± 8.56 μm for 0.1 ml·h^{-1}, 0.87 ± 0.24, and 3.79 ± 1.86 μm for 0.5 ml·h^{-1} and 3.02 ± 0.95 and 14.02 ± 6.59 μm for 1.0 ml·h^{-1}, see Fig. 5 **(a-c)**. The average ratio between short fiber length-to-diameter was 9.42 ± 6.62 (0.1 ml·h^{-1}), 4.58 ± 2.46 (0.5 ml·h^{-1}), and 4.99 ± 2.79 (1.0 ml·h^{-1}), respectively. All results were presented and summarized as bar graphs, histograms, and cluster plots in Fig. 5 **(d – g) and** Table S1 in the SI. Similar results were obtained by producing a short PMMA electrospun with a decreasing polymer flow rate, explained as the effect of the entanglement loss of the polymer jet mechanism, contributing to rapid polymer chain disentanglement.[31] In other work, the increasing flow rate from 0.0012 to 0.0280 ml·h^{-1} resulted in CA short fibers with a length from ~ 65 to ~ 150 um.[28] However, above 0.030 ml·h^{-1}, the electrospinning was transferred to continuous fibers production.

We produced fibers with low, 0.1 ml·h^{-1}, medium, 0.5 ml·h^{-1}, and high, 1.0 ml·h^{-1} polymer solution flow rates. As discussed earlier, short fiber production can be prevented by increasing a polymer flow rate.[28,31] In this work, 0.5 ml·h^{-1} gives the smallest fiber – 0.87 ± 0.24 μm in diameter and 3.79 ± 1.86 μm in length. Importantly, polymer solution flow allows controlling the short fibers' dimensions, increasing the aspect ratio by approximately 200 % (from ~ 5 to ~ 10) rather than the applied voltage or distance from the collector.

3.3.4. Electrical field effect on short fibers size

As stated before, the electric field, and its strength are determining factors of the electrospinning process. The electric field strength in electrospinning depends mainly on two values: applied voltage and the distance between the needle and the collector, see Table 1. Several studies show that increasing the electric field strength makes it possible to change the fiber diameter, mat thickness, and morphology and improve the mechanical properties of the fibers.[54,63,64] However, some studies show that an increase in the electric field does not always reduce fiber diameter, which depends on the polymer solution, type of collector, or substrate used.[65] In addition, changing the distance and electric field significantly affects the solvent evaporation rate, consequently leading to a change in fiber diameter.[66] Here, we include data from all variations in applied voltage and nozzle-to-collector distance. Short electrospun PMMA fibers were produced using produced with 0.45 (SF1), 0.68 (SF2), 0.85 (SF5), 1.04 (SF3), and 1.53 (SF4) kV·cm^{-1} electrical field strength, see Fig. 6**.** The average diameters and lengths of the fibers varied depending on the electrical field strength conditions, see Table S1. All results were presented and summarized as bar graphs, histograms, and cluster plots in Fig. 6 **(f – i) and** Table S1 in the SI. The resulting short fibers range from 0.8 to 3.8 μm in diameter and 1 to 15 μm in length, depending on the electric field strength. However, as for nozzle-to-collector distance, an increasing electric field strength from 0.45 to 1.53 kV·cm^{-1} does not lower a short fiber diameter or length. The smallest ~ 0.87 μm in diameter and ~ 3.79 μm in length short fibers were obtained at 1.04 kV·m^{-1} (SF3), and the biggest ~ 2.85 μm and the longest ~ 15.44 μm for 0.85 kV·m^{-1} (SF5), see Table S1. For this work, changing the electric field's strength significantly affects the diameters and lengths of the short fibers.

3.4. Analysis of results based on scaling laws

In this part of the paper, an attempt is made to generalize the experimental results obtained with theoretical values. The scaling law allows us to approximate the length and diameter of electrospun short fibers when polymer flow rate, electric field strength, solvent quality, polymerization rate, and polymer volume fraction are known.[31] For length, the following equation was used:

$$L_{SL} \approx v_0^{1.4} E^{-1.1} N^{3.9} k^{2.1} \phi^{7.5} \quad (1)$$

where ν_0 is the initial jet velocity, E is electric field strength, k is the solvent quality, N is the degree of polymerization, and ϕ is the polymer volume fraction. The diameter of short fibers was expressed as:

$$D_{SL} \approx v_0^{0.1} E^{-0.07} N^{-0.4} k^{-0.2} \phi^{0.19} \quad (2)$$

The rest of the formulas used for calculations are included in the SI, see. Table S2.

In the case of eq. (1) and (2), the parameters affecting fiber length and diameter are ν_0 and E, where k, N, and ϕ are constant. Fig. 7 shows the values for L_{SL} and D_{SL} concerning specific values of the electric field strength E at constant Q (0.5 ml·h^{-1}) and to L_f and R_f obtained experimentally. The difference between the experimental results and the predicated via scaling law is presented in Fig. 7. Increasing the strength of the electric field in the case of L_{SL} results in a decrease in length and has no noticeable effect on short fiber diameters. For experimental results, the electric field strength influenced both values, i.e., length and diameter (L_f and D_f), but this is not a linear relation. As mentioned earlier, for specific values, a rise in the electric field strength causes an increase and/or a decrease in the diameter or length of the short fibers.

Notably, the main differences between the experimental and the predicted results based on the scaling laws eq. (1) and (2) are related to the having evaporation rate, boiling point, and vapor pressure of solvents impacting Maxwell stresses generated during electrospinning.[67] Therefore, a type of solvent (good or θ-solvent) used for the process is essential in electrospinning short fibers. In a study [31], the solvent system for PMMA was based on chloroform and DMF. Chloroform is characterized by a higher evaporation rate and lower boiling point than DMF.[68] However, in the case of our results where only DMF is used as a solvent, the eq. (1) and (2) show the discrepancy in short fibers' predicted length and diameter. In our studies, a high fraction of PMMA (52 %) was used.[68] Importantly, the experimental and predicted results fall within the same order of magnitude for fiber length, as shown in

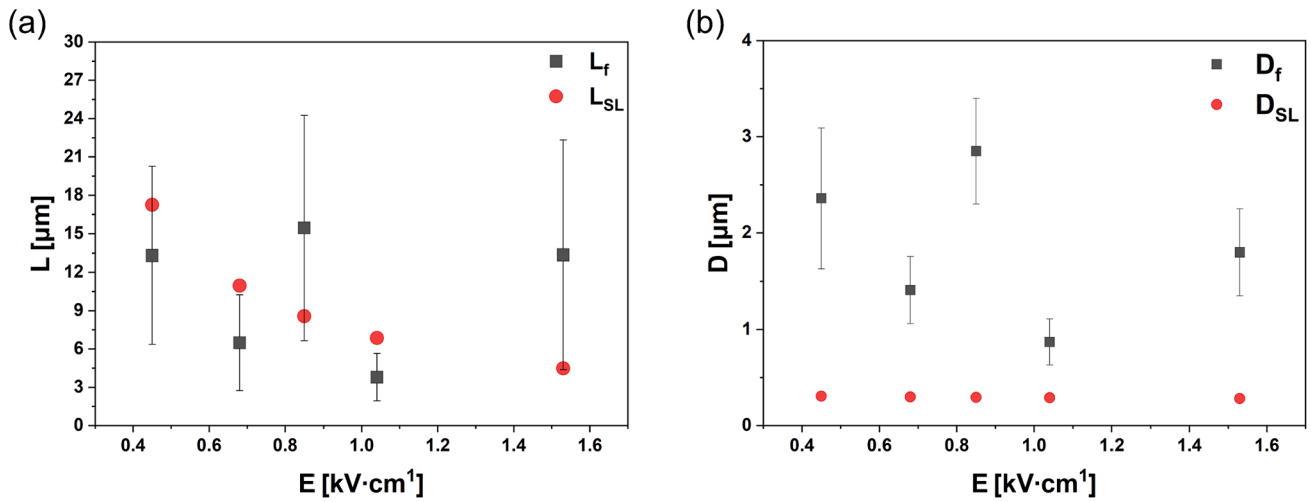

Fig. 7. The correlation between the obtained experimental results (L_f, D_f) and the predicted with the scaling laws (L_{SL} and D_{SL}) using eq. (1) and (2), (a) the length, L, and (b) diameter, D, of short fibers.

Fig. 7 **(a)**.

3.5. Comparison of short fiber aspect ratio

Short fibers' aspect ratio and length are crucial parameters defining the short fiber's usefulness in composite applications.[30] In the case of short fibers, their ability to transfer stress is determined by critical fiber length, which depends on the tensile strength of the short fiber, the fiber diameter, and the fiber–matrix bond strength.[69] Typically, the composite's embedded fibers must be 8 to 20 times bigger than the critical fiber length to achieve a reinforcing effect. Longer fibers and a high aspect ratio can reduce the mechanical properties of the composite.[70] However, using fibers with a very high aspect ratio can lead to processing difficulties, such as breakage during mixing and poor fiber dispersion.[71] This can result in the formation of agglomerates, which can reduce the mechanical properties of the composite.[72].

In the case of this work, we obtained short PMMA fibers with the narrowest length spread and the smallest aspect ratio that could be obtained for direct electrospinning compared to previously shown results in the literature, see Fig. 8. We can also control fiber diameter using different electrospinning parameters, which is impossible during homogenization. Summarizing this work, Fig. 9 is the cluster graph showing the results D_f and L_f for chopped fibers over 60 min and direct electrospinning of short fibers at voltage U = 23 kV, flow rate Q = 0.5 ml·h^{-1} and distance between the nozzle and the collector Y = 22 cm, (sample SF3 in Table 1). The dimensions of directly electrospun short fibers are well controlled, as we show that the obtained results are less scattered than the standard way of chopping fibers, such as homogenization. Indeed, this work indicates clear advantages of manufacturing short micron-sized fibers in direct electrospinning, opening a new perspective for producing short fibers for various nanotechnologies and reinforced composites applications.

3.6. DSC and FT-IR analysis

The thermal and spectroscopy analysis of PMMA samples was performed to verify structural changes in electrospun continuous fibers after homogenization and short fibers produced via direct electrospinning. The DSC analysis is presented in Fig. S1 in the SI. Glass transition (T_g) temperature or pure PMMA powder, continuous fibers, and chopped fibers for 10, 30, and 60 min were evaluated, see Fig. S1 **(a)** in the SI reaching very similar temperatures: 128.6 ± 0.5, 129.7 ± 0.5, 130.9 ± 1.3, 131 ± 0.6, and 132.5 ± 0.6 °C, respectively. The T_g value aligns with the literature value for PMMA with M_w = 350 000 g·mol^{-1}.[73] No specific points are visible in the heating curves, indicating an effect of the homogenization process or the homogenization medium, such as water or ethanol, on the structure of the short fibers. The T_g was 94.6 ± 1.8 °C for PMMA' powder and around ~ 98 °C for SF1 − 7 short fibers samples, see Fig. S1 **(b)** in the SI, similar to the previously reported results.[73] In summary, the homogenization medium and electrospinning parameters do not affect the structure of short PMMA fibers.

Fourier transform infrared spectroscopy (FT-IR) of PMMA samples results are presented in Fig. S2 in the SI, indicating peaks at 1145, 1189, 1241 cm^{-1} for C–O–C stretching vibration and 1387 cm^{-1}, 749 cm^{-1} due to the α-methyl group vibrations. The peaks presented at 855, 977, and 1063 cm^{-1} are for characteristic absorption vibration of PMMA. The 1431 cm^{-1} band is a bending vibration of the C–H bonds and –CH3 group. The band at 1718 cm^{-1} is related to the presence of the acrylate carboxyl group, and 2985 cm^{-1}, and 2948 cm^{-1} are present due to the C–H bond stretching vibrations, respectively. The last two absorption peaks can be observed at 1593 cm^{-1} and 3658 cm^{-1}, which is attributed to the stretching of the –OH group caused by absorbed moisture.[74]. All FT-IR spectra are in Fig. S2 in the SI. Similar to DSC results, no significant differences were found in FT-IR spectra's all short PMMA fibers regardless of the manufacturing method. In addition, no extra peaks were noticed in the DSC curves or FT-IR spectra, which could show residues of DMF in the produced material.

3.7. Potential applications and perspectives

As stated in the introduction, current methods of producing short fibers result in high values with a large spread in aspect ratio, limiting the application of this type of material. However, in this work, we show it is possible to obtain regular (low spread in diameter and length) polymer short fibers in the aspect ratio range of approximately 4 to 10, which opens many new perspectives for using these materials. In Fig. 10 an example of applications of short electrospun fibers are schematically presented. On of them are polymer sponges, where short electrospun polymer fibers can be used to produce them.[75–78] However, the mechanical cutting of continuous electrospun fibers were used causing irregularities and defects in the structure of the sponge.[79,80] Hydrogel, exhibiting poor mechanical properties, take the advantage of short electrospun polymer fibers.[81–83] This reinforcement improves cells' growth and enhance hydrogel's mechanical properties.[84,85] The direct electrospun short fibers embedded into a hydrogel matrix, improved even biocompatibility of hydrogel.[86] In pharmaceutics and drug delivery systems, short fibers offer promise in enhancing drug efficacy and minimizing side effects. Shin *et al.* presented short and

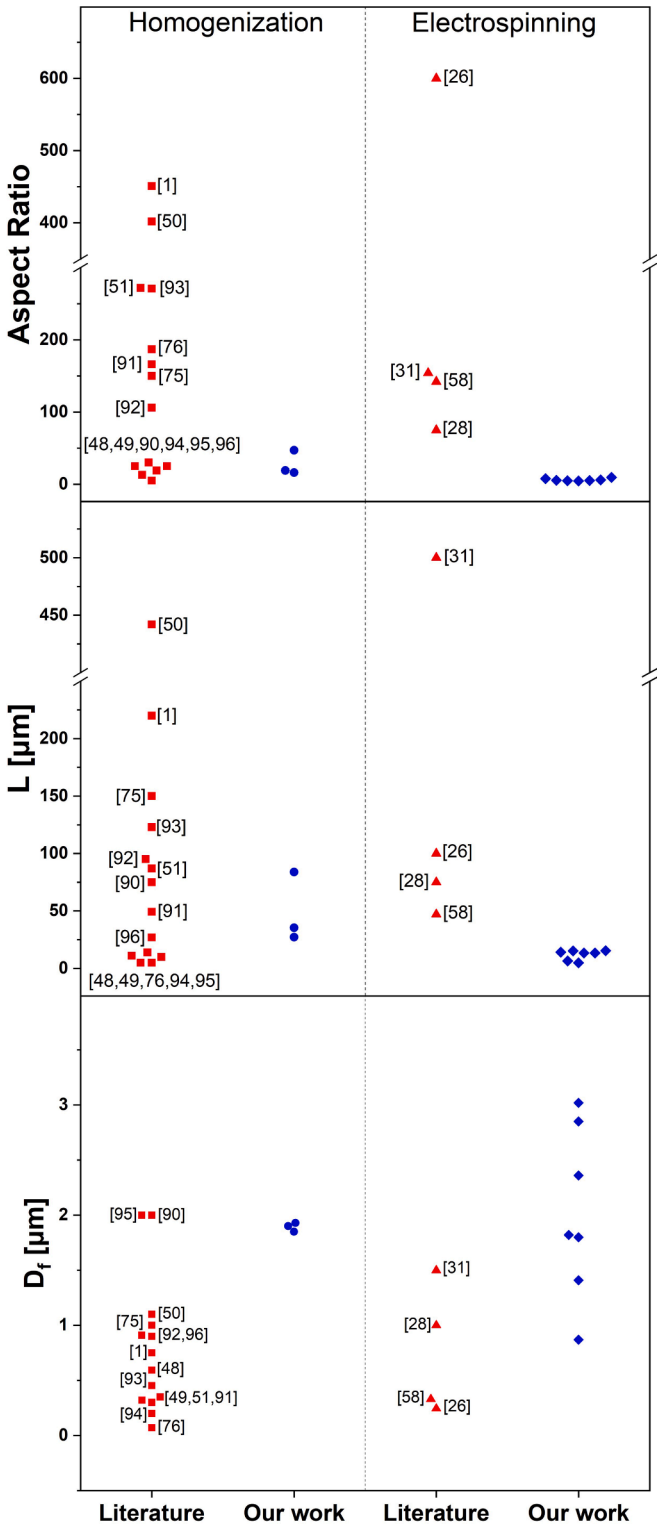

Fig. 8. Data comparison of average aspect ratio, length, and fiber diameter of homogenized (chopped) and electrospun short fibers taken from the literature (red points – reference number in bracket) to values achieved in our work (blue points). Literature data were . (For interpretation of the references to colour in this figure legend, the reader is referred to the web version of this article.) adopted from [1,26,28,31,48–51,58,75,76,90–96]

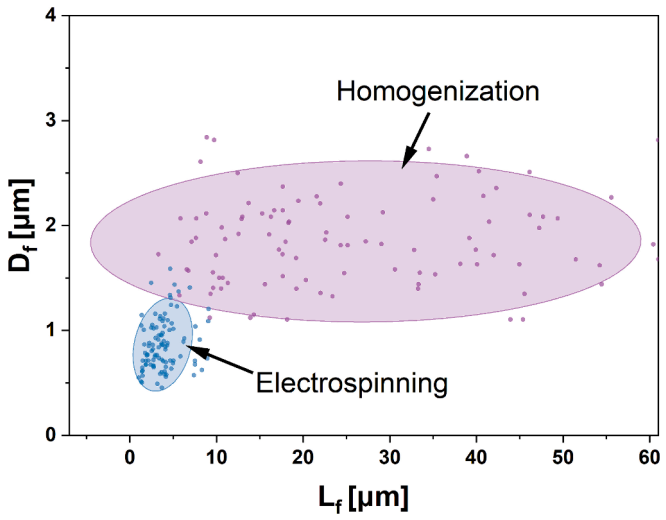

Fig. 9. Cluster plot indicating the diameter D_f and the length L_f of fibers regimes for directly electrospun short and chopped fibers over 60 min of homogenization.

injectable polylactic acid fibers for enhancing T-cell function.[87] Similar results of particle shape effect on T-cells were observed in other works.[88,89] Generally, short fiber composites play a crucial role in increasing the strength and stiffness of materials. While short fibers have a lower length-to-diameter ratio compared to continuous fibers, their effective utilization depends on factors such as fiber orientation and adhesion between interfaces. The primary role of fibers in composite materials is to bear the load, resulting in increased strength, modulus, and stiffness. The ability to transfer stress in the short fibers composites is determined by the critical length, which depends mainly on diameter and length, which can be controlled during the electrospinning.[69].

4. Conclusion

This work focused on showing the strategies for direct electrospinning of short polymer fibers. We have demonstrated that it is possible to control the size, diameter, and length of short fibers by adjusting electrospinning parameters such as applied voltage, distance, or polymer solution flow rate. Before the processing, the essential first step is selecting a polymer with the lowest possible molecular weight, which in this case was M_w = 15 000 g·mol^{-1} and maintaining the polymer concentration at around 52 % for PMMA. We highlighted the differences in the dynamics of polymer solution jet during electrospinning of short and continuous fibers. To create short fibers via electrospinning, the whipping of jets is omitted, and short jets are formed.

We obtained short fibers via direct electrospinning with a narrow fiber length and aspect ratio. Additionally, we show that changing an electrospinning parameter like a nozzle-to-collector distance or polymer flow rate doubles the short fiber aspect ratio (from 4.58 to 9.42). It is possible to obtain fibers dimensions below 1 µm in diameter and around 4 µm in length to a few microns in diameter and around 14 µm in length. The scaling laws verification was performed to predict the dimensions of short fibers for selected solvent combinations. Additionally, the application areas for electrospun short fibers were presented. In conclusion, electrospinning is an accurate and precise method that allows for the controlled production of short fibers without the need for the additional post-treatment or mechanical cutting.

CRediT authorship contribution statement

Daniel P. Ura: Data curation, Formal analysis, Funding acquisition, Investigation, Methodology, Project administration, Resources,

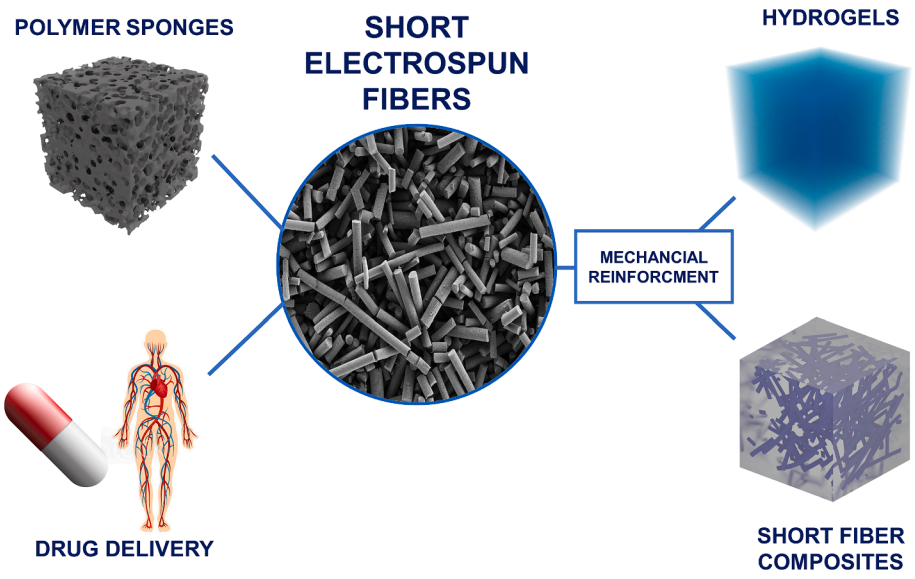

Fig. 10. Application areas for short fibers produced via electrospinning.

Validation, Writing – original draft, Writing – review & editing. **Urszula Stachewicz:** Conceptualization, Funding acquisition, Methodology, Project administration, Resources, Supervision, Visualization, Writing – original draft, Writing – review & editing.

Declaration of competing interest

The authors declare that they have no known competing financial interests or personal relationships that could have appeared to influence the work reported in this paper.

Data availability

Data will be made available on request.

Acknowledgements

This study was conducted as part of the Preludium 20 project granted by the National Science Centre in Poland, No. 2021/41/N/ST5/01804, and the thermal and the spectroscopy analyses within BioCom4SavEn project funded by the European Research Council under the European Union's Horizon 2020 Framework Programme for Research and Innovation (ERC grant agreement no. 948840).

Appendix A. Supplementary data

Supplementary data to this article can be found online at https://doi.org/10.1016/j.compositesa.2024.108138.

References

[1] Zhang X, Geven MA, Grijpma DW, Gautrot JE, Peijs T. Polymer-polymer composites for the design of strong and tough degradable biomaterials. Mater Today Commun 2016;8:53–63. https://doi.org/10.1016/j.mtcomm.2016.05.001.
[2] Shah V, Bhaliya J, Patel GM, Deshmukh K. Advances in polymeric nanocomposites for automotive applications: a review. Polym Adv Technol 2022;33:3023–48. https://doi.org/10.1002/pat.5771.
[3] Snowdon MR, Mohanty AK, Misra M. Miscibility and performance evaluation of biocomposites made from polypropylene/poly(lactic acid)/poly(hydroxybutyrate-cohydroxyvalerate) with a sustainable biocarbon filler. ACS Omega 2017;2:6446–54. https://doi.org/10.1021/acsomega.7b00983.
[4] Jiang L, Zhou Y, Jin F. Design of short fiber-reinforced thermoplastic composites: a review. Polym Compos 2022;43:4835–47. https://doi.org/10.1002/pc.26817.
[5] Lotfi A, Li H, Dao DV, Prusty G. Natural fiber–reinforced composites: a review on material, manufacturing, and machinability. J Thermoplast Compos Mater 2019;34:1–47. https://doi.org/10.1177/0892705719844546.
[6] Kerni L, Singh S, Patnaik A, Kumar N. A review on natural fiber reinforced composites. Mater Today Proc 2020;28:1616–21. https://doi.org/10.1016/j.matpr.2020.04.851.
[7] Maiti S, Islam MR, Uddin MA, Afroj S, Eichhorn SJ, Karim N. Sustainable fiber-reinforced composites: a review. Adv Sustain Syst 2022:6. https://doi.org/10.1002/adsu.202200258.
[8] Liu H, Gough CR, Deng Q, Gu Z, Wang F, Hu X. Recent advances in electrospun sustainable composites for biomedical, environmental, energy, and packaging applications. Int J Mol Sci 2020;21:1–23. https://doi.org/10.3390/ijms21114019.
[9] Karbowniczek JE, Ura DP, Stachewicz U. Nanoparticles distribution and agglomeration analysis in electrospun fiber based composites for desired mechanical performance of poly(3-hydroxybuty-rate-co-3-hydroxyvalerate (PHBV) scaffolds with hydroxyapatite (HA) and titanium dioxide (TiO2) towards medical applications. Compos B Eng 2022;241:110011. https://doi.org/10.1016/j.compositesb.2022.110011.
[10] Kamarudin SH, Mohd Basri MS, Rayung M, Abu F, Ahmad S, Norizan MN, et al. A review on natural fiber reinforced polymer composites (NFRPC) for sustainable industrial applications. Polymers (Basel) 2022;14:1–36. https://doi.org/10.3390/polym14173698.
[11] Prashanth S, Subbaya K, Nithin K, Sachhidananda S. Fiber reinforced composites - a review. Journal of Material Science & Engineering 2017:06. https://doi.org/10.4172/2169-0022.1000341.
[12] Yoo DY, Lee JH, Yoon YS. Effect of fiber content on mechanical and fracture properties of ultra high performance fiber reinforced cementitious composites. Compos Struct 2013;106:742–53. https://doi.org/10.1016/j.compstruct.2013.07.033.
[13] Khalid MY, Al Rashid A, Arif ZU, Ahmed W, Arshad H, Zaidi AA. Natural fiber reinforced composites: sustainable materials for emerging applications. Results in Engineering 2021;11:100263. https://doi.org/10.1016/j.rineng.2021.100263.
[14] Bernasconi A, Cosmi F, Hine PJ. Analysis of fibre orientation distribution in short fibre reinforced polymers: a comparison between optical and tomographic methods. Compos Sci Technol 2012;72:2002–8. https://doi.org/10.1016/j.compscitech.2012.08.018.
[15] Jauhari N, Mishra R, Thakur H. Natural fibre reinforced composite laminates – a review. Mater Today Proc 2015;2:2868–77. https://doi.org/10.1016/j.matpr.2015.07.304.
[16] Kim D, Lee J, Nomura T, Dede EM, Yoo J, Min S. Topology optimization of functionally graded anisotropic composite structures using homogenization design method. Comput Methods Appl Mech Eng 2020;369:113220. https://doi.org/10.1016/j.cma.2020.113220.
[17] Niemczyk-Soczynska B, Dulnik J, Jeznach O, Kolbuk D, Sajkiewicz P. Shortening of electrospun PLLA fibers by ultrasonication. Micron 2021;145:103066. https://doi.org/10.1016/j.micron.2021.103066.
[18] Papkov D, Zou Y, Andalib MN, Goponenko A, Cheng SZD, Dzenis YA. Simultaneously strong and tough ultrafine continuous nanofibers. ACS Nano 2013;7:3324–31. https://doi.org/10.1021/nn400028p.
[19] Arinstein A, Burman M, Gendelman O, Zussman E. Effect of supramolecular structure on polymer nanofibre elasticity. Nat Nanotechnol 2007;2:59–62. https://doi.org/10.1038/nnano.2006.172.
[20] Jiang S, Chen Y, Duan G, Mei C, Greiner A, Agarwal S. Electrospun nanofiber reinforced composites: a review. Polym Chem 2018;9:2685–720. https://doi.org/10.1039/c8py00378e.
[21] Reneker DH, Yarin A, Zussman E, Koombhongse S, Kataphinan W. Nanofiber manufacturing: Toward better process. Control 2006. https://doi.org/10.1021/bk-2006-0918.ch002.

[22] Reneker DH, Yarin AL, Fong H, Koombhongse S. Bending instability of electrically charged liquid jets of polymer solutions in electrospinning. J Appl Phys 2000;87:4531–47. https://doi.org/10.1063/1.373532.

[23] Wang C, Cheng YW, Hsu CH, Chien HS, Tsou SY. How to manipulate the electrospinning jet with controlled properties to obtain uniform fibers with the smallest diameter?-a brief discussion of solution electrospinning process. J Polym Res 2011;18:111–23. https://doi.org/10.1007/s10965-010-9397-1.

[24] Hekmati AH, Rashidi A, Ghazisaeidi R, Drean JY. Effect of needle length, electrospinning distance, and solution concentration on morphological properties of polyamide-6 electrospun nanowebs. Text Res J 2013;83:1452–66. https://doi.org/10.1177/0040517512471746.

[25] Theron SA, Zussman E, Yarin AL. Experimental investigation of the governing parameters in the electrospinning of polymer solutions. Polymer (Guildf) 2004;45:2017–30. https://doi.org/10.1016/j.polymer.2004.01.024.

[26] Fathona IW, Yabuki A. One-step fabrication of short electrospun fibers using an electric spark. J Mater Process Technol 2013;213:1894–9. https://doi.org/10.1016/j.jmatprotec.2013.05.013.

[27] Yabuki A, Motonobu E, Fathona IW. Controlling the length of short electrospun polymer nanofibers via the addition of micro-spherical silica particles. J Mater Sci 2017;52:4016–24. https://doi.org/10.1007/s10853-016-0663-4.

[28] Fathona IW, Yabuki A. A simple one-step fabrication of short polymer nanofibers via electrospinning. J Mater Sci 2014;49:3519–28. https://doi.org/10.1007/s10853-014-8065-y.

[29] Fathona IW, Yabuki A. Mapping the influence of electrospinning parameters on the morphology transition of short and continuous nanofibers. Fibers Polym 2016;17:1238–44. https://doi.org/10.1007/s12221-016-6241-1.

[30] Ura DP, Berniak K, Stachewicz U. Critical length reinforcement in core-shell electrospun fibers using composite strategies. Compos Sci Technol 2021;211:108867. https://doi.org/10.1016/j.compscitech.2021.108867.

[31] Greenfeld I, Zussman E. Polymer entanglement loss in extensional flow: evidence from electrospun short nanofibers. J Polym Sci B Polym Phys 2013;51:1377–91. https://doi.org/10.1002/polb.23345.

[32] Frazer RQ, Byron RT, Osborne PB, West KP. PMMA: an essential material in medicine and dentistry. J Long Term Eff Med Implants 2012;15:629–39. https://doi.org/10.1615/jlongtermeffmedimplants.v15.i6.60.

[33] Ali U, Karim KJBA, Buang NA. A review of the properties and applications of poly (methyl methacrylate) (PMMA). Polym Rev 2015;55:678–705. https://doi.org/10.1080/15583724.2015.1031377.

[34] Zucchelli A, Focarete ML, Gualandi C, Ramakrishna S. Electrospun nanofibers for enhancing structural performance of composite materials. Polym Adv Technol 2011;22:339–49. https://doi.org/10.1002/pat.1837.

[35] Estaji S, Paydayesh A, Mousavi SR, Khonakdar HA, Abiyati MM. Polycarbonate/poly(methyl methacrylate)/silica aerogel blend composites for advanced transparent thermal insulations: mechanical, thermal, and optical studies. Polym Compos 2021;42:5323–34. https://doi.org/10.1002/pc.26226.

[36] Mazov IN, Kuznetsov VL, Moseenkov SI, Ishchenko AV, Romanenko AI, Anikeeva OB, et al. Electrophysical and electromagnetic properties of pure MWNTs and MWNT/PMMA composite materials depending on their structure. Fullerenes, Nanotubes, Carbon Nanostruct 2010;18:505–15. https://doi.org/10.1080/1536383X.2010.488184.

[37] Alzarrug FA, Dimitrijević MM, Jančić Heinemann RM, Radojević V, Stojanović DB, Uskoković PS, et al. The use of different alumina fillers for improvement of the mechanical properties of hybrid PMMA composites. Mater Des 2015;86:575–81. https://doi.org/10.1016/j.matdes.2015.07.069.

[38] Prahasanti C, Nugraha AP, Kharisma VD, Ansori ANM, Ridwan RD, Putri TPS, et al. A bioinformatic approach of hydroxyapatite and polymethylmethacrylate composite exploration as dental implant biomaterial. J Pharm Pharmacogn Res 2021;9:746–54. https://doi.org/10.56499/jppres21.1078_9.5.746.

[39] Su KH, Su CY, Cho CT, Lin CH, Jhou GF, Chang CC. Development of thermally conductive polyurethane composite by low filler loading of spherical BN/PMMA composite powder. Sci Rep 2019;9:3–10. https://doi.org/10.1038/s41598-019-50985-5.

[40] Salih SI, Oleiwi JK, Mohamed AS. Investigation of mechanical properties of PMMA composite reinforced with different types of natural powders. ARPN Journal of Engineering and Applied Sciences 2018;13:8889–900.

[41] Yin Z, Hannard F, Barthelat F. Impact-resistant nacre-like transparent materials. Science 1979;2019(364):1260–3.

[42] Liao X, Hu P, Agarwal S, Greiner A. Impact of the fiber length distribution on porous sponges originating from short electrospun fibers made from polymer yarn. Macromol Mater Eng 2020;305:1–6. https://doi.org/10.1002/mame.201900629.

[43] Lauricella M, Succi S, Zussman E, Pisignano D, Yarin AL. Models of polymer solutions in electrified jets and solution blowing. Rev Mod Phys 2020;92:35004. https://doi.org/10.1103/RevModPhys.92.035004.

[44] Luo CJ, Stride E, Edirisinghe M. Mapping the influence of solubility and dielectric constant on electrospinning polycaprolactone solutions. Macromolecules 2012;45:4669–80. https://doi.org/10.1021/ma300656u.

[45] Tao G, Chen Y, Mu J, Zhang L, Ye C, Li W. Exploring the entangled state and molecular weight of UHMWPE on the microstructure and mechanical properties of HDPE/UHMWPE blends. J Appl Polym Sci 2021;138:1–9. https://doi.org/10.1002/app.50741.

[46] Bentley FE, Passieux R, David L, Osorio-Madrazo A. Pure chitosan biomedical textile fibers from mixtures of low-and high-molecular weight bidisperse polymer solutions: processing and understanding of microstructure-mechanical properties' relationship. Int J Mol Sci 2022;23. https://doi.org/10.3390/ijms23094767.

[47] Shakil UA, Abu Hassan S, Bin YMY, Rejab MRM. A focused review of short electrospun nanofiber preparation techniques for composite reinforcement. Nanotechnol Rev 2022;11:1991–2014. https://doi.org/10.1515/ntrev-2022-0116.

[48] Yoshikawa C, Zhang K, Zawadzak E, Kobayashi H. A novel shortened electrospun nanofiber modified with a "concentrated" polymer brush. Sci Technol Adv Mater 2011;12. https://doi.org/10.1088/1468-6996/12/1/015003.

[49] Xu W, Feng Y, Ding Y, Jiang S, Fang H, Hou H. Short electrospun carbon nanofiber reinforced polyimide composite with high dielectric permittivity. Mater Lett 2015;161:431–4. https://doi.org/10.1016/j.matlet.2015.09.014.

[50] Drummer M, Liang C, Kreger K, Rosenfeldt S, Greiner A, Schmidt HW. Stable mesoscale nonwovens of electrospun polyacrylonitrile and interpenetrating supramolecular 1,3,5-benzenetrisamide fibers as efficient carriers for gold nanoparticles. ACS Appl Mater Interfaces 2021;13:34818–28. https://doi.org/10.1021/acsami.1c06442.

[51] Langner M, Greiner A. Wet-laid meets electrospinning: nonwovens for filtration applications from short electrospun polymer nanofiber dispersions. Macromol Rapid Commun 2016;37:351–5. https://doi.org/10.1002/marc.201500514.

[52] Lokesh P, Surya Kumari TSA, Gopi R, Loganathan GB. A study on mechanical properties of bamboo fiber reinforced polymer composite. Mater Today Proc 2020;22:897–903. https://doi.org/10.1016/j.matpr.2019.11.100.

[53] Kammoun S, Doghri I, Adam L, Robert G, Delannay L. First pseudo-grain failure model for inelastic composites with misaligned short fibers. Compos Part A Appl Sci Manuf 2011;42:1892–902. https://doi.org/10.1016/j.compositesa.2011.08.013.

[54] Mu X, Zheng Y, Xin B. Effects of the electric field distribution on electrospun PET fibers properties. J Phys Conf Ser 2021;1790. https://doi.org/10.1088/1742-6596/1790/1/012059.

[55] Ura DP, Knapczyk-Korczak J, Szewczyk PK, Sroczyk EA, Busolo T, Marzec MM, et al. Surface potential driven water harvesting from fog. ACS Nano 2021;15:8848–59. https://doi.org/10.1021/acsnano.1c01437.

[56] Ura DP, Rosell-Llompart J, Zaszczyńska A, Vasilyev G, Gradys A, Szewczyk PK, et al. The role of electrical polarity in electrospinning and on the mechanical and structural properties of as-spun fibers. Materials 2020;13:4169. https://doi.org/10.3390/ma13184169.

[57] Sun Z, Zussman E, Yarin AL, Wendorff JH, Greiner A. Compound core-shell polymer nanofibers by co-electrospinning. Adv Mater 2003;15:1929–32. https://doi.org/10.1002/adma.200305136.

[58] Fathona IW, Yabuki A. Short electrospun composite nanofibers: effects of nanoparticle concentration and surface charge on fiber length. Curr Appl Phys 2014;14:761–7. https://doi.org/10.1016/j.cap.2014.03.015.

[59] Singh YP, Dasgupta S, Nayar S, Bhaskar R. Optimization of electrospinning process & parameters for producing defect-free chitosan/polyethylene oxide nanofibers for bone tissue engineering. J Biomater Sci Polym Ed 2020;31:781–803. https://doi.org/10.1080/09205063.2020.1718824.

[60] Zhang H. Effects of electrospinning parameters on morphology and diameter of electrospun PLGA/MWNTs fibers and cytocompatibility in vitro. J Bioact Compat Polym 2011;26:590–606. https://doi.org/10.1177/0883911511424015.

[61] Zargham S, Bazgir S, Tavakoli A, Rashidi AS, Damerchely R. The effect of flow rate on morphology and deposition area of electrospun nylon 6 nanofiber. J Eng Fiber Fabr 2012;7:42–9. https://doi.org/10.1177/155892501200700414.

[62] Tang XP, Si N, Xu L, Liu HY. Effect of flow rate on diameter of electrospun nanoporous fibers. Therm Sci 2014;18:1447–9. https://doi.org/10.2298/TSCI1405447T.

[63] Jin S, Xin B, Zheng Y, Liu S. Effect of electric field on the directly electrospun nanofiber yarns: simulation and experimental study. Fibers Polym 2018;19:116–24. https://doi.org/10.1007/s12221-018-7734-2.

[64] Yang Y, Jia Z, Liu J, Li Q, Hou L, Wang L, et al. Effect of electric field distribution uniformity on electrospinning. J Appl Phys 2008;103. https://doi.org/10.1063/1.2924439.

[65] Xie S, Zeng Y. Effects of electric field on multineedle electrospinning: Experiment and simulation study. Ind Eng Chem Res 2012;51:5336–45. https://doi.org/10.1021/ie2020763.

[66] Cai Y, Gevelber M. The effect of relative humidity and evaporation rate on electrospinning: fiber diameter and measurement for control implications. J Mater Sci 2013;48:7812–26. https://doi.org/10.1007/s10853-013-7544-x.

[67] Reznik SN, Yarin AL, Theron A, Zussman E. Transient and steady shapes of droplets attached to a surface in a strong electric field. J Fluid Mech 2004;516:349–77. https://doi.org/10.1017/S0022112004000679.

[68] Nuamcharoen P, Kobayashi T, Potiyaraj P. Influence of volatile solvents and mixing ratios of binary solvent systems on morphology and performance of electrospun poly(vinylidene fluoride) nanofibers. Polym Int 2021;70:1465–77. https://doi.org/10.1002/pi.6218.

[69] Mortazavian S, Fatemi A. Effects of fiber orientation and anisotropy on tensile strength and elastic modulus of short fiber reinforced polymer composites. Compos B Eng 2015;72:116–29. https://doi.org/10.1016/j.compositesb.2014.11.041.

[70] Abu Al-Rub RK, Ashour AI, Tyson BM. On the aspect ratio effect of multi-walled carbon nanotube reinforcements on the mechanical properties of cementitious nanocomposites. Constr Build Mater 2012;35:647–55. https://doi.org/10.1016/j.conbuildmat.2012.04.086.

[71] Danso H, Martinson DB, Ali M, Williams J. Effect of fibre aspect ratio on mechanical properties of soil building blocks. Constr Build Mater 2015;83:314–9. https://doi.org/10.1016/j.conbuildmat.2015.03.039.

[72] Chen L, Yu Q, Wang Y, Li H. BisGMA/TEGDMA dental composite containing high aspect-ratio hydroxyapatite nanofibers. Dent Mater 2011;27:1187–95. https://doi.org/10.1016/j.dental.2011.08.403.

[73] Lin T, Li Y, Wang J, You J. Effect of PMMA molecular weight on its localization during crystallization of PVDF in their blends. Polymers (Basel) 2021;13:1–12. https://doi.org/10.3390/polym13234138.
[74] Duan G, Zhang C, Li A, Yang X, Lu L, Wang X. Preparation and characterization of mesoporous zirconia made by using a poly (methyl methacrylate) template. Nanoscale Res Lett 2008;3:118–22. https://doi.org/10.1007/s11671-008-9123-7.
[75] Duan G, Jiang S, Moss T, Agarwal S, Greiner A. Ultralight open cell polymer sponges with advanced properties by PPX CVD coating. Polym Chem 2016;7:2759–64. https://doi.org/10.1039/c6py00339g.
[76] Jiang S, Reich S, Uch B, Hu P, Agarwal S, Greiner A. Exploration of the electrical conductivity of double-network silver nanowires/polyimide porous low-density compressible sponges. ACS Appl Mater Interfaces 2017;9:34286–93. https://doi.org/10.1021/acsami.7b11740.
[77] Cheong JY, Mafi M, Benker L, Zhu J, Mader M, Liang C, et al. Ultralight, structurally stable electrospun sponges with tailored hydrophilicity as a novel material platform. ACS Appl Mater Interfaces 2020;12:18002–11. https://doi.org/10.1021/acsami.0c03103.
[78] Xu T, Li X, Liang Z, Amar VS, Huang R, Shende RV, et al. Carbon nanofibrous sponge made from hydrothermally generated biochar and electrospun polymer nanofibers. Advanced Fiber Materials 2020;2:74–84. https://doi.org/10.1007/s42765-020-00032-0.
[79] Liu M, Duan X-P, Li Y-M, Yang D-P, Long Y-Z. Electrospun nanofibers for wound healing. Mater Sci Eng C 2017;76:1413–23. https://doi.org/10.1016/j.msec.2017.03.034.
[80] Xu T, Ding Y, Liang Z, Sun H, Zheng F, Zhu Z, et al. Three-dimensional monolithic porous structures assembled from fragmented electrospun nanofiber mats/membranes: methods, properties, and applications. Prog Mater Sci 2020;112:100656. https://doi.org/10.1016/j.pmatsci.2020.100656.
[81] Lin X, Zhao X, Xu C, Wang L, Xia Y. Progress in the mechanical enhancement of hydrogels: fabrication strategies and underlying mechanisms. J Polym Sci 2022;60:2525–42. https://doi.org/10.1002/pol.20220154.
[82] Li Y, Wang J, Wang Y, Cui W. Advanced electrospun hydrogel fibers for wound healing. Compos B Eng 2021;223:109101. https://doi.org/10.1016/j.compositesb.2021.109101.
[83] Xu T, Liu K, Sheng N, Zhang M, Liu W, Liu H, et al. Biopolymer-based hydrogel electrolytes for advanced energy storage/conversion devices: properties, applications, and perspectives. Energy Storage Mater 2022;48:244–62. https://doi.org/10.1016/j.ensm.2022.03.013.
[84] Wang M, Du J, Li M, Pierini F, Li X, Yu J, et al. In situ forming double-crosslinked hydrogels with highly dispersed short fibers for the treatment of irregular wounds. Biomater Sci 2023:2383–94. https://doi.org/10.1039/d2bm01891h.
[85] Poveda-Reyes S, Mellera-Oglialoro LR, Martínez-Haya R, Gamboa-Martínez TC, Gõmez Ribelles JL, Gallego FG. Reinforcing an injectable gelatin hydrogel with PLLA microfibers: two routes for short fiber production. Macromol Mater Eng 2015;300:977–88. https://doi.org/10.1002/mame.201500033.
[86] Regev O, Reddy CS, Nseir N, Zussman E. Hydrogel reinforced by short albumin fibers: mechanical characterization and assessment of biocompatibility. Macromol Mater Eng 2013;298:283–91. https://doi.org/10.1002/mame.201200012.
[87] Shin HM, Ju Y, Kim G, Lee JW, Seo MW, Sim JH, et al. Recyclable cytokines on short and injectable polylactic acid fibers for enhancing T-cell function. Adv Funct Mater 2019;29:1–11. https://doi.org/10.1002/adfm.201808361.
[88] Oh J, Xia X, Wong WKR, Wong SHD, Yuan W, Wang H, et al. The effect of the nanoparticle shape on T cell activation. Small 2022;18:1–16. https://doi.org/10.1002/smll.202107373.
[89] Meyer RA, Sunshine JC, Perica K, Kosmides AK, Aje K, Schneck JP, et al. Biodegradable nanoellipsoidal artificial antigen presenting cells for antigen specific T-cell activation. Small 2015;11:1519–25. https://doi.org/10.1002/smll.201402369.
[90] Kriha O, Becker M, Lehmann M, Kriha D, Krieglstein J, Yosef M, et al. Connection of hippocampal neurons by magnetically controlled movement of short electrospun polymer fibers - a route to magnetic micromanipulators. Adv Mater 2007;19:2483–5. https://doi.org/10.1002/adma.200601937.
[91] Feng ZQ, Shi C, Zhao B, Wang T. Magnetic electrospun short nanofibers wrapped graphene oxide as a promising biomaterials for guiding cellular behavior. Mater Sci Eng C 2017;81:314–20. https://doi.org/10.1016/j.msec.2017.08.015.
[92] Xu T, Liang Z, Ding B, Feng Q, Fong H. Polymer blend nanofibers containing polycaprolactone as biocompatible and biodegradable binding agent to fabricate electrospun three-dimensional scaffolds/structures. Polymer (Guildf) 2018;151:299–306. https://doi.org/10.1016/j.polymer.2018.07.074.
[93] Xu T, Zheng F, Chen Z, Ding Y, Liang Z, Liu Y, et al. Halloysite nanotubes sponges with skeletons made of electrospun nanofibers as innovative dye adsorbent and catalyst support. Chem Eng J 2019;360:280–8. https://doi.org/10.1016/j.cej.2018.11.233.
[94] Deniz AE, Celebioglu A, Kayaci F, Uyar T. Electrospun polymeric nanofibrous composites containing TiO2 short nanofibers. Mater Chem Phys 2011;129:701–4. https://doi.org/10.1016/j.matchemphys.2011.06.018.
[95] Thieme M, Agarwal S, Wendorff JH, Greiner A. Electrospinning and cutting of ultrafine bioerodible poly(lactide-co-ethylene oxide) tri- and multiblock copolymer fibers for inhalation applications. Polym Adv Technol 2011;22:1335–44. https://doi.org/10.1002/pat.1617.
[96] Li Y, Wang J, Qian D, Chen L, Mo X, Wang L, et al. Electrospun fibrous sponge via short fiber for mimicking 3D ECM. J Nanobiotechnology 2021;19:1–15. https://doi.org/10.1186/s12951-021-00878-5.